Chemical Engineering Journal Advances 25 (2026) 101046

Contents lists available at ScienceDirect

Chemical Engineering Journal Advances

journal homepage: www.sciencedirect.com/journal/chemical-engineering-journal-advances

Degradation and defluorination of perfluorooctane sulfonate (PFOS) forever chemical in water using hydrodynamic cavitation treatment

Amit Kumar [a,*], Anett Georgi [b], Ysabel Huaccallo-Aguilar [a,*], Markus Meier [c], Holger Kryk [a], Sebastian Felix Reinecke [a], Uwe Hampel [a,d]

[a] Clean Water Technology Lab (CLEWATEC), Institute of Fluid Dynamics, Helmholtz Zentrum Dresden-Rossendorf, Bautzner Landstrasse 400 01328 Dresden, Germany
[b] Helmholtz Centre for Environmental Research – UFZ, Department Technical Biogeochemistry, 04318 Leipzig, Germany
[c] AIR LIQUIDE Forschung und Entwicklung GmbH, Gwinnerstraße 27-33, 60388 Frankfurt, Germany
[d] Technische Universität Dresden, Chair of Imaging Techniques in Energy and Process Engineering, Dresden 01062, Germany

ARTICLE INFO

Keywords:
Long-chain PFAS
Hydrodynamic cavitation
PFOS
Degradation and defluorination
Energy efficiency
Treatment chain

ABSTRACT

Per- and polyfluoroalkyl substances (PFAS), also known as "forever chemicals," are persistent environmental contaminants that pose significant risks to human health and aquatic ecosystems. Their extreme chemical stability primarily due to the strong carbon–fluorine (C–F) bond, the strongest bond in organic chemistry makes them highly resistant to degradation, even under harsh oxidative conditions. This study examines the degradation and defluorination of PFAS using a catalyst-free and chemical-additive-free orifice-based hydrodynamic cavitation (HC) treatment system. In HC, the rapid formation and subsequent collapse of cavitation bubbles generate intense shockwaves, localized high pressures, and elevated temperatures. These extreme conditions create a highly reactive physicochemical environment capable of initiating PFAS breakdown and promoting effective defluorination. In this study, perfluorooctane sulfonate (PFOS), a representative long-chain PFAS, was selected at initial concentrations of 1 mg/L and 5 mg/L. Treatments were conducted under intense HC conditions (inlet orifice pressure of 48 bar; cavitation number of 0.03) with varying treatment durations. The results demonstrated increased PFOS degradation with treatment time along with detection of released fluoride ions indicating effective cleavage of C–F bonds. PFOS degradation reached 37%, and the degree of defluorination was 20% related to initial PFOS, respectively. The degradation followed first-order kinetics, with rate constants ranging from 0.7×10^{-3} to 40×10^{-3} 1/min. At an electrical energy per order (*EEO*) of 7–598 kWh/m^3/order, the corresponding electrical energy input required for PFOS degradation ranged from 1 to 75 kWh/m^3. These findings underscore the potential of HC as a scalable and effective PFAS treatment technology.

1. Introduction

Per- and polyfluoroalkyl substances (PFAS) are a large and structurally diverse class of over 14,000 synthetic fluorochemicals widely used in industrial and consumer products (as shown in Fig. 1a) due to their hydrophobicity, oleophobicity, and chemical stability [1–3]. Their extreme persistence has led to widespread environmental contamination, particularly in water sources, raising significant public health and ecological concerns [4,5]. PFAS are highly mobile in aquatic environments, bioaccumulative, and have been linked to a range of adverse health effects, including endocrine disruption, liver toxicity, immune suppression, and developmental delays. Studies have found PFAS in the blood of ~97% of the U.S. population, including fetuses, indicating transplacental transfer [6,7]. Emerging evidence also suggests that PFAS exposure may alter DNA methylation in children, with implications for immune function, metabolism, and neurodevelopment [8].

PFAS are highly resistant to thermal, chemical, and biological degradation due to the exceptional strength of the carbon–fluorine bond (~485 kJ/mol), which is stronger than most other single bonds (as shown in Fig. 1b), making them extremely persistent in the environment [9–11]. Some PFAS (e.g. PFOS, perfluorooctanoic acid: PFOA and perfluorohexanesulfonate: PFHxS) can take more than a thousand years to break down under natural conditions [12,13]. The conventional wastewater treatment plants (WWTPs) are often ineffective at removing them and can even act as secondary sources of PFAS emissions [6]. PFAS contamination is globally pervasive, with detections in drinking water,

* Corresponding authors.
E-mail addresses: a.kumar@hzdr.de (A. Kumar), y.huaccallo-aguilar@hzdr.de (Y. Huaccallo-Aguilar).

https://doi.org/10.1016/j.ceja.2026.101046

Available online 16 January 2026

groundwater, sediments, and even in wildlife from remote regions such as the Arctic [14]. In response, regulatory actions are being implemented. The European Union's revised Drinking Water Directive (EU 2020/2184) sets enforceable limits for PFAS in drinking water, requiring member states to meet thresholds of 500 ng/L for total PFAS or 100 ng/L for a group of 20 specific compounds by January 2026 [14,15]. While only a limited number of PFAS have been banned at the EU level so far, and some EU countries have recommended broader bans, wider restrictions are currently under regulatory review [16].

With growing recognition of PFAS contamination as a critical environmental crisis, there is an urgent need for effective remediation strategies [17,18]. Current treatment methods such as adsorption onto activated carbon, ion exchange, and membrane filtration primarily focus on sequestration rather than degradation, leading to secondary waste streams that require further management [19]. For example, high-temperature incineration (~1000 °C) is commonly used to destroy PFAS-containing waste [20]. However, the incineration approach is costly and may lead to incomplete combustion or partial defluorination [18,21]. Advanced oxidation and reduction processes (AOPs and ARPs), including, cold plasma, sulfate radical-based degradation, photolysis, sonolysis, electrochemical oxidation, and other related approaches have been explored for PFAS treatment [17,22,23]. Although these methods demonstrate strong potential for breaking down PFAS, several challenges remain. Many of these methods still generate transformation by-products, only a limited number have been evaluated at large scale, and several approaches are highly energy-intensive, making their application to real wastewater effluents difficult. Scalability and operational cost therefore remain major barriers to practical implementation.

HC is a promising and scalable approach for wastewater treatment [27,31–33]. It has been tested for the degradation of emerging contaminants such as pharmaceuticals, dyes, and industrial chemicals, and has also shown potential for PFAS degradation [28,29]. HC operates by rapidly forming and collapsing vapor bubbles due to pressure fluctuations, releasing tremendous energy that produces high-velocity microjets, shock waves, and microturbulence. These phenomena generate extreme, transient physicochemical conditions, including localized temperatures exceeding 5000°C and pressures of several hundred atmospheres (Fig. 1c) [28,31]. Numerous studies have investigated bubble radius dynamics, transient temperature and pressure profiles during bubble collapse, and their relevance to chemical degradation processes [34–37]. Bubble implosion generates intense thermal and mechanical effects, leading to the formation of highly reactive species (especially hydroxyl radicals: HO•, hydrogen atom radicals: H•, solvated electrons:

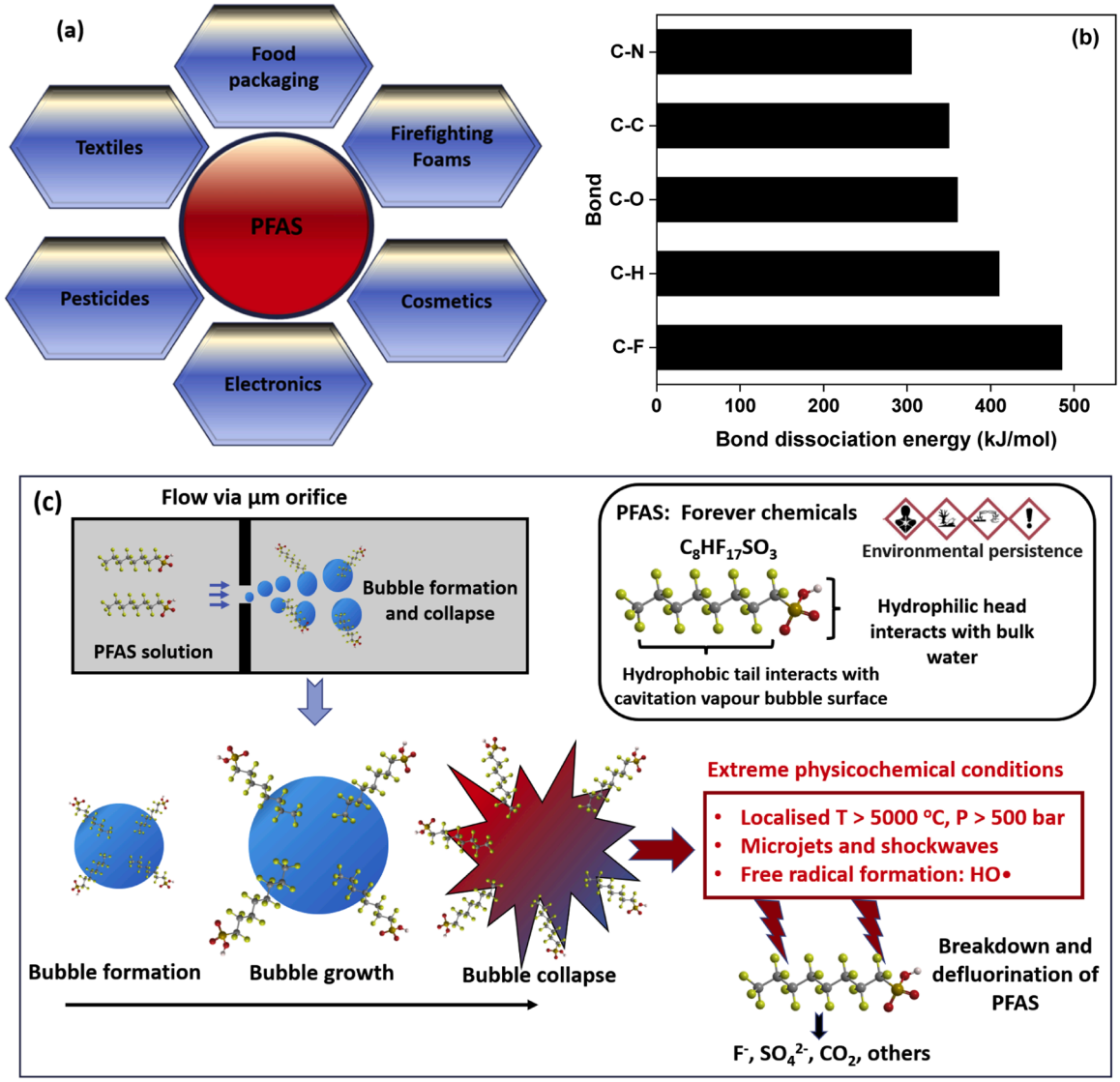

Fig. 1. (a) Representative consumer and industrial products containing PFAS [24]. (b) Bond dissociation energies of relevant single bonds [25,26]. (c) Schematic illustration of cavitation bubble formation and collapse via HC, highlighting the resulting physical environment and proposed PFAS degradation pathways [27–30].

e_{sol}, etc.), which contribute to PFAS degradation and defluorination. PFAS molecules, due to their surfactant nature, tend to accumulate at the bubble–liquid interface during cavitation [28,29,38,39]. Their hydrophobic fluorinated tail preferentially aligns toward the bubble interface, while the hydrophilic head group (e.g., $–SO_3^-$) remains in the aqueous phase, stabilizing the molecule at the interface [40,41].

During HC, PFOS degradation primarily takes place through pyrolytic decomposition caused by the extreme, localized high temperatures and pressures generated during bubble collapse [28,29]. The degradation can occur in three main regions. First, inside the bubble, very high temperatures and pressures promote thermal cleavage and the formation of reactive species such as HO•. Second, at the bubble–liquid interface, the temperatures although lower than inside the bubble are still high enough to enable thermal decomposition of PFOS. Third, in the bulk liquid, longer-lived reactive species formed at the interface can further degrade the intermediate products. The degradation and defluorination occur mainly at the bubble–liquid interface, where PFOS is exposed to intense thermal and chemical conditions, enabling pyrolysis or thermolysis [28,41]. PFOS itself does not react efficiently with HO• because its C–F bonds are highly stable. However, once PFOS is fragmented by cavitation-driven thermal effects, it can generate reactive intermediate products. Therefore, although HO• alone cannot cleave the C–F bonds, they play an important role in degrading PFOS intermediates formed after initial thermal fragmentation and thus mineralization [10,28,29].

Previous studies on PFAS degradation using HC are very limited. To date, only a few investigations have addressed this topic. One study examined the degradation of PFAS mixtures, including PFOS, at trace concentrations in the ng/L range (e.g., around 2 ng/L) [28]. Another study focused on the degradation of PFOA using HC combined with activated persulfate at initial concentrations between 0.5 and 10 mg/L [29]. These studies demonstrated that HC could induce both degradation and partial defluorination of PFAS molecules. In particular, Wang et al [29] reported the formation of shorter-chain PFAS intermediates following HC treatment of PFOA, either alone or in combination with persulfate, indicating stepwise breakdown of the parent compound. Among cavitation-based processes, acoustic cavitation (AC) has been extensively studied for PFAS degradation; however, HC offers several key advantages, including lower treatment costs, greater system size flexibility, and improved scalability. Most existing PFAS degradation studies focus on environmentally relevant trace levels (ng/L to μg/L) typically found in surface water and groundwater. In contrast, this study addresses higher PFAS concentrations representative of concentrated waste streams, such as concentrates of membrane filtration or regeneration solutions from adsorption processes (e.g. electrosorption), aqueous film-forming foams (AFFF), industrial discharges, and landfill leachate. Furthermore, quantification of fluoride release which is relevant for degradation verification requires working in the mg/L PFAS concentration range as trace fluoride quantification is difficult.

In this work, the experimental investigation was carried out using an orifice-type HC system to evaluate PFAS degradation and defluorination in a tap water matrix. The HC process offers a chemical-, catalyst- and waste-free treatment strategy. Leveraging the extreme physical and chemical conditions created during cavitation events, our approach specifically targets long-chain PFAS such as PFOS, one of the most persistent and recalcitrant compounds within the PFAS family. Treatment variables included reaction time, number of passes through the HC reactor, and initial PFOS concentration, all under a constant inlet pressure of 48 bar. Fluoride ion release was used as a primary indicator of C–F bond cleavage, providing quantitative insight into degradation efficiency. In addition, *EEO*, energy consumption and treatment cost (in € per m^3 of PFOS-treated water) were estimated and compared with existing PFAS remediation technologies. This work advances the development of scalable, sustainable HC-based solutions for PFAS treatment and offers a promising pathway for addressing the growing environmental and regulatory challenges posed by these persistent pollutants.

2. Materials and methods

2.1. PFOS sample preparation

A stock solution of PFOS (purchased from Sigma-Aldrich, ≥ 98% purity) was prepared by dissolving it in tap water at an initial concentration of 200 mg/L. This stock solution was then diluted with tap water to achieve the desired working concentrations of 1 mg/L and 5 mg/L. In this study, most of the treatment experiments were conducted using an initial PFOS concentration of 5 mg/L to assess its degradation efficiency. The initial PFOS solution also contained PFHxS as an impurity or precursor at a low concentration of 4 μg/L (at 5 mg/L of PFOS). Compared to PFOS, PFHxS is a shorter-chain PFAS (C = 6) classified as an anionic fluorosurfactant, known for its high persistence and ability to bioaccumulate in organisms [28]. Due to its presence, PFHxS was also included as a target contaminant in the analysis. The physicochemical properties of PFOS, existing concentrations in the environment, aquatic systems, human body, and food, as well as their impacts, are shown in Supplementary Material Table A.1 [3,42–45].

2.2. Hydrodynamic cavitation setup

Fig. 2(a) illustrates the experimental setup used for PFOS degradation via HC. A high-pressure reciprocating pump (Novados H3, AxFlow) was employed to circulate the PFOS solution from the feed tank through a stainless-steel pipe (6 mm outer diameter, 4 mm inner diameter) toward a laser-drilled orifice (200 μm). A pressure gauge (manometer: Afriso, 0-100 bar) and pressure sensor (RS PRO Pressure Sensor, 160 bar Max, Gauge Reading) were installed upstream of the orifice to monitor inlet pressure, providing both manual and real-time digital readings to ensure accurate control of cavitation conditions. Flow rate through the orifice was measured using a flow meter (Bronkhorst, ES-FLOW). The solution pH (SMARTPAT PH 8570, Krohne, sensor) and temperature were continuously monitored. Treated samples were collected in tubes and stored in the refrigerator at low temperature for analysis.

Fig. 2(b) shows the HC based PFAS treatment system, which can operate at flow rates of up to 100 L/h. The red-circled section highlights the cavitation module containing the orifice nozzle used to generate cavitation. The orifice configuration was selected because the abrupt pressure drop and high-velocity liquid jet passing the orifice create highly intense HC [24,37,38]. This localized cavitation generates strong shear forces, microjets, and reactive species that can effectively degrade PFAS, including PFOS. Orifice plates are widely used in HC systems due to their simplicity, reproducibility, and energy efficiency, as well as their ability to produce a well-defined cavitation region. Although other cavitation geometries, such as venturi nozzles or rotor–stator systems, are also capable of generating HC, the orifice-based setup was chosen for its operational simplicity and for its ability to achieve high local cavitation intensities making it particularly suitable for studying PFOS degradation.

Fig. 2(c) is a close-up view of the nozzle with the orifice at the top. As fluid passes through the orifice, the local pressure drops below the liquid vapor pressure, leading to cavitation bubble formation. The transparent window allows real-time monitoring of cavitation activity and flow behaviour. Fig. 2(d) shows an image captured using a high-speed Phantom 710 L camera (equipped with a Tokina Macro ATX Pro 100 mm f/2.8 lens and illuminated by a Veritas 120 E LED lamp with 12 diodes), depicting the cavitation bubblecloud formed as fluid passes through the orifice. This visualization provides valuable insight into the flow characteristics and cavitation dynamics. It was also found that even after long experimental durations, no clogging of the orifice was observed. The orifice was tested under both conditions PFOS treatment in tap water and treatment of other contaminants spiked into real wastewater samples from municipal wastewater treatment plants [32,

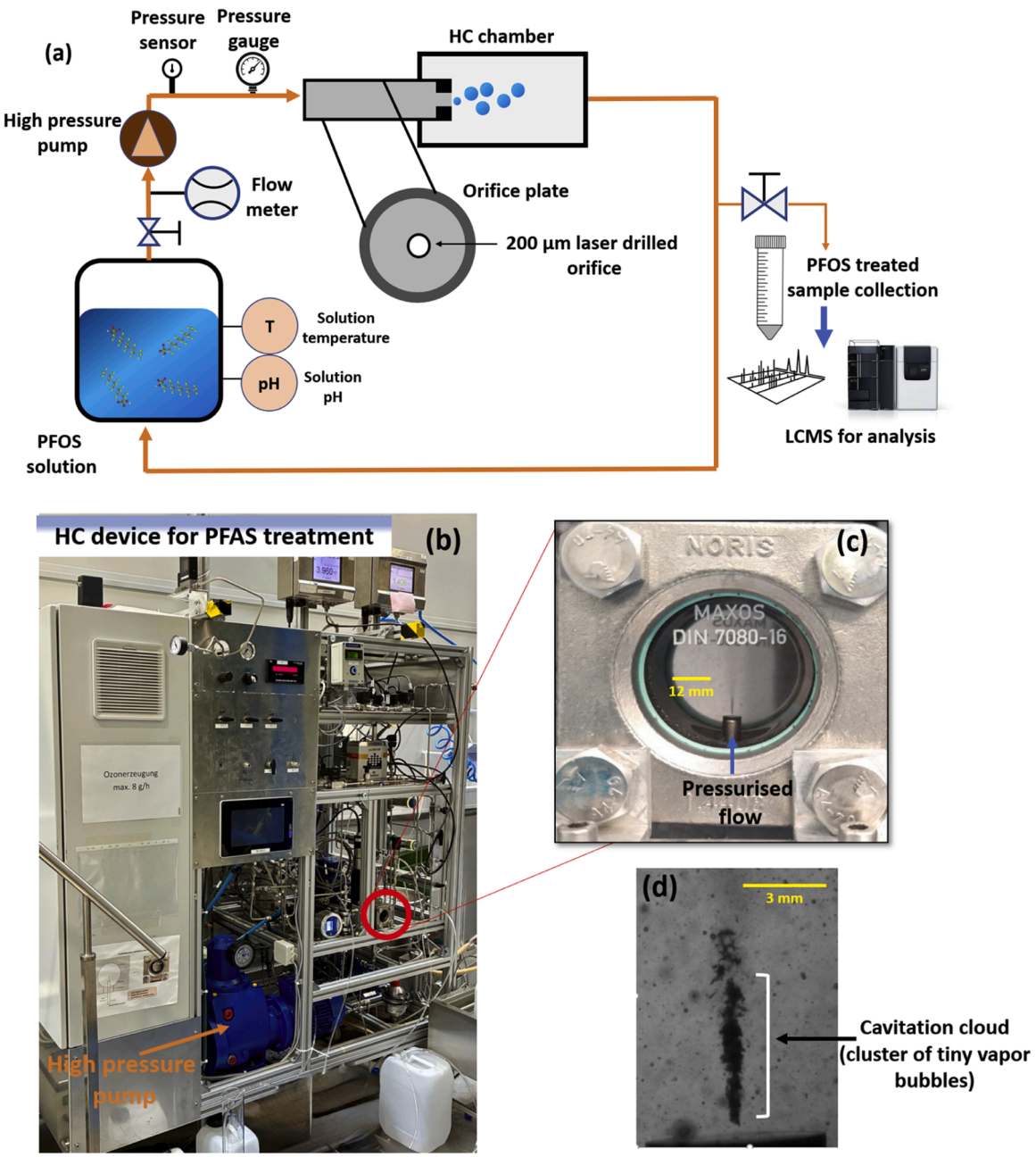

Fig. 2. (a) Schematic of the experimental setup. (b) PFOS treatment system. (c) HC chamber featuring the orifice plate. (d) High-speed imaging of cavitation captured at 72000 frames per second.

33].Analytics for PFOS samples.

2.3. *Analytics for PFOS samples*

PFOS and its C4-C8 perfluorocarboxylate degradation intermediates, *i.e.,* PFBA (C4), PFPeA (C5), PFHeA (C6), PFHpA(C7) and PFOA (C8), were determined with an HPLC-MS system (SHIMADZU Corporation; LCMS-2020). The mobile phase consisted of solvents A and B: solvent A was composed of 20 mM ammonium acetate in 10 vol% methanol and 90 vol% deionized water and solvent B was composed of 20 mM ammonium acetate in 10 vol% deionized water and 90 vol% methanol. A mixture consisting of 65 vol% of solvent B and 35 vol% of solvent A was pumped with a flow rate of 0.25 mL/min. The run time of each measurement was 28 min. The detection limit of this method is 0.6 µg/L for PFOS, 0.2 µg/L for PFHxS and in the range of 0.2 µg/L to 2 µg/L for the remaining PFAS analyzed and the standard deviation is within 2% of the mean value. The standard deviation of the HPLC-MS results, expressed as a percentage of the mean value, is shown in Supplementary Material (Table A.2). PFOS and PFHxS concentrations as a function of treatment time, with error bars indicating measurement uncertainty, shown in Supplementary Material (Fig. A.1)

Fluoride concentrations were analyzed using the Spectroquant® Fluoride test reagent (Supelco, 1.17236.0001). Fluoride ions react with part of an arsenic-free red zirconium-dye solution to form a colorless complex, which in turn results in a bleaching of the red color (SPADNS method). The concentration of the unconsumed zirconium-dye solution is subsequently determined photometrically at 575 nm. The method is analogous to USEPA 340.1. Samples containing 0.1 to 2 mg/L fluoride were mixed with the SPADNS reagent solution in a volume ratio of 10:1 and the absorbance was measured after 20 min.

2.4. PFOS treatment conditions

The treatment of PFOS using HC was carried out under well-defined flow and operational parameters, as detailed in Table 1. Cavitation was generated at a high inlet pressure of 48 bar, achieving a flow rate of 8.9 L/h, which resulted in a pressure drop indicative of favourable conditions for bubble formation and collapse. Experiments were conducted at temperature of 22 °C and a neutral to slightly basic pH of 8.07, using 0.5 L of the PFOS solution. The temperature of the liquid was measured throughout the treatments and remained nearly constant. The experiments were performed in continuous recirculation mode with multiple number of passes and treatment times of up to 240 min. Five treated samples were collected at intervals of 30, 60, 120, 180, and 240 min.

2.5. Analysis of obtained experimental data

The following parameters and equations were used to analyze the experimental data, as shown in Table 2. Each formula, along with a description of its significance and the definitions of relevant variables, is provided below.

The cavitation number is a dimensionless parameter used to characterize the intensity of cavitation. A lower C_v indicates stronger cavitation conditions. The terms used in its calculation are defined as follows: P_{rec} (N/m^2), the pressure measured at the recovery region after the orifice; P_{vap} (N/m^2), the liquid vapor pressure at the operating temperature; ρ, the liquid density (kg/m^3); and v_o, the velocity at the orifice (m/s).

The Reynolds number (*Re*) is a dimensionless value used to predict flow patterns in fluid dynamics. High *Re* value indicates turbulent flow, which is desirable for effective cavitation.μ represents dynamic viscosity of the liquid (Pa·s).

The degradation efficiency (%) of PFOS during treatment was calculated by comparing the initial concentration ($[PFOS]_o$) and the concentration at time *t* ($[PFOS]_t$,mg/L). Defluorination was calculated to quantify the extent to which fluorine atoms bound in PFOS molecules are released as inorganic fluoride ions (F^-). The percentage defluorination reflects the degree of PFOS mineralization, indicating how much of the fluorine content was successfully recovered $[TF]_o$ represents total fluorine content (mol/L) initially present in the PFOS compound.

The net amount of F^- released during the degradation process was calculated, indicating the release of fluorine atoms from PFAS breakdown into the aqueous phase. Here, $[F]_t^-$ represent the molar fluoride concentration at time *t*, and $[F^-]_o$ denotes the initial molar fluoride concentration in tap water.

The F^- mass recovery quantifies the proportion of total fluorine encountering both the measured inorganic fluoride ions released ($[F^-]_t$) and the theoretically estimated fluorine still bound in PFOS molecules present at a given time ($[TF]_t$) relative to the initial total fluorine content. The recovery metric ensures mass balance by accounting for both released and residual fluorine, offering insight into the extent of PFOS degradation and the efficiency of fluoride recovery. time *t*.

The degradation kinetics of PFOS was evaluated by monitoring its concentration over time during treatment. The data were fitted to a first-order kinetic model, which showed the best fit based on the regression constant (R^2). This model allows for the determination of the degradation rate constant (k_1), indicating how rapidly PFOS is degraded under the applied conditions (k_1: first-order PFOS degradation rate constant, 1/min). To express the degradation rate of PFOS in terms of $1/N_p$, the first-order rate constant equation was modified by replacing *t* with N_p, resulting in a corresponding rate constant, k_2, expressed in terms of 1/Np (k_2: first-order degradation rate constant, $1/N_p$).

HP was calculated to represent the energy required by the pump to drive the PFOS solution through the system, based on the pressure difference between the orifice inlet and ambient conditions, as well as the flow rate. The parameters used in the calculation are defined as follows: P_o is the pressure measured at the orifice inlet, $P_{ambient}$ is the ambient pressure (both expressed in N/m^2), and Q_o is the volumetric flow rate (expressed in m^3/s).

The *EEO*, a log-reduction-based efficiency metric, was calculated to express the energy required to reduce the PFOS concentration by one order of magnitude in one cubic meter of water. This metric allows for the comparison of energy efficiency among different treatment processes, system configurations, and operational scales. The parameters used in the calculation are defined as follows: V_S is the treated volume (m^3), and $[PFOS]_o$ and $[PFOS]_t$ represent the initial concentration and the concentration at time *t* (mg/L), respectively.

Energy yield (in mg/kWh), a mass-based removal efficiency metric, was calculated to represent the amount of PFAS specifically PFOS removed per kilowatt-hour of energy consumed. It is used to compare the efficiency of treatment systems in terms of mass removal. This metric reflects the removal efficiency relative to energy input; a higher energy

Table 1
Flow conditions during the PFOS treatment by HC.

	Notation	Values
Inlet pressure at orifice	P_o (bar)	48
Flow at orifice	Q_o (L/h)	8.9
Orifice size	D_o (μm)	200
Fluid velocity at orifice	v_o (m/s)	78.69
Reynolds number	R_e	15.74×10^3
Cavitation number	C_v	0.032
Sample temperature	T (°C)	22
pH of PFOS solution	pH	8.07
Sample volume	V_s (L)	0.5
Number of passes via HC	N_p	0 to 71
Time per pass	t_p (min)	3.37
Hydraulic power	*HP* (W)	9.36
Hydraulic retention time	*HRT* (min)	11 to 92

Table 2
Mathematical formulas used for the analysis of the obtained experimental data.

Parameters	Formula
C_v	$C_v = \frac{P_{rec} - P_{vap}}{\frac{1}{2} \times \rho \times v_o^2}$
R_e	$R_e = \frac{\rho \times v_o \times D_o}{\mu}$
PFOS degradation, %	$\frac{[PFOS]_o - [PFOS]_t}{[PFOS]_o} \times 100$
Defluorination, %	$\frac{[F^-]_t - [F^-]_o}{[TF]_o} \times 100$
F^- yield, μg/L	$[F^-]_t$-$[F^-]_o$
F^- mass recovery, %	$\frac{[F^-]_t + [TF]_t}{[F^-]_o + [TF]_o} \times 100$
Degradation kinetics of PFOS	$\frac{[PFOS]_t}{[PFOS]_o} = e^{-k_1 t}$
Degradation rate of PFOS in terms of $1/N_p$	$\frac{[PFOS]_{N_p}}{[PFOS]_o} = e^{-k_2 N_p}$
HP, W	$(P_o - P_{ambient}) \times Q_o$
The electrical energy per order, *EEO in* kWh/m^3/order	$\frac{HP\ (kW) \times \text{treatment time (h)}}{V_s\ (m^3) \times \log(\frac{[PFOS]_o}{[PFOS]_t})}$
Energy yield, mg/kWh	$\frac{[PFOS]_o \left(\frac{mg}{L}\right) \times V_s\ (L) \times \text{PFOS degradation \%} \times \frac{1}{100}}{HP\ (kW) \times \text{treatment time (h)}}$
Energy input, kWh/m^3	$\frac{HP\ (kW) \times \text{treatment time (h)}}{V_s\ (m^3)}$
Cost, €/m^3	$\frac{HP\ (kW) \times \text{treatment time (h)}}{V_s\ (m^3)} \times 0.2889\ (€/kWh)$
HRT, min	$\frac{\text{HC chamber volume (L)}}{Q_o\ (\frac{L}{min})}$
N_p	$N_p = \frac{Q_o\ (\frac{L}{h})}{V_s\ (L)} \times \text{treatment time (h)}$
PFOS degradation per pass, %	$\frac{\text{Change in degradation \%}}{\text{Change in number of passes}}$

yield indicates a more efficient process with potentially lower operational costs for contaminant removal. However, it needs to be mentioned that energy yield in case of first-order kinetics processes is highly affected by the initial target compound concentration.

Energy input (kWh/m^3), a volume-based cost metric, was determined as the total electrical energy required to treat one cubic meter of water. It provides an estimate of the overall treatment cost per unit volume and serves as a basis for cost estimation and preliminary benchmarking of the process. The cost in euros (€) per cubic meter for PFAS treatment using HC was calculated based on energy consumption. The unit price for industrial electricity was considered using the EU average electricity rate (current rate of conversion) of ~€0.2889 per kWh.

HRT represents the actual time that the PFOS-containing solution spends inside the HC chamber during a single pass. It is a critical parameter, as it determines how long the fluid is exposed to cavitation-induced physical and chemical effects, which drive pollutant degradation.

The number of passes N_p refers to how many times the entire volume of the solution circulates through the cavitation device, including the feed tank and connecting pipes, during the treatment process. It provides insight into the cumulative exposure of target pollutants to cavitation effects. A higher N_p typically indicates increased contact with the cavitation field, potentially enhancing degradation. The degradation per pass is calculated for each interval between consecutive pass counts.

3. Results and discussion

3.1. PFOS degradation and defluorination

In this work, cavitation was generated at P_o of 48 bar, and the corresponding C_v defined as the ratio of the static pressure deficit to the dynamic pressure was calculated as 0.032. A C_v less than 1 generally indicates conditions favourable for cavitation inception, while significantly lower C_v values correspond to more intense transient cavitation [27,28,46]. Under such conditions, bubble collapse produces extremely high localized temperatures and pressures, enhancing PFOS degradation through pyrolytic cleavage and the formation of reactive species. At $C_v \approx 0.032$, the system operates in a strong cavitation regime where PFOS destruction can occur predominantly via localized pyrolysis at or near the bubble interface, in combination with radical-driven oxidation of intermediate fragments. Previous HC studies on organic pollutants consistently report that lower cavitation numbers lead to more violent bubble collapse and higher degradation efficiencies [27,46,47]. Our own prior investigations on succinic acid removal and the degradation of persistent pharmaceuticals similarly demonstrated improved degradation performance at lower C_v values [32,33].

The R_e was calculated to be 15.74×10^3, indicating turbulent flow through the orifice. This turbulent flow promotes rapid bubble collapse and efficient energy transfer, which can enhance mixing and cavitation intensity. High-speed imaging, shown in Fig. 2(d), captured a cavitation cloud emerging from the orifice, composed of numerous tiny bubbles.

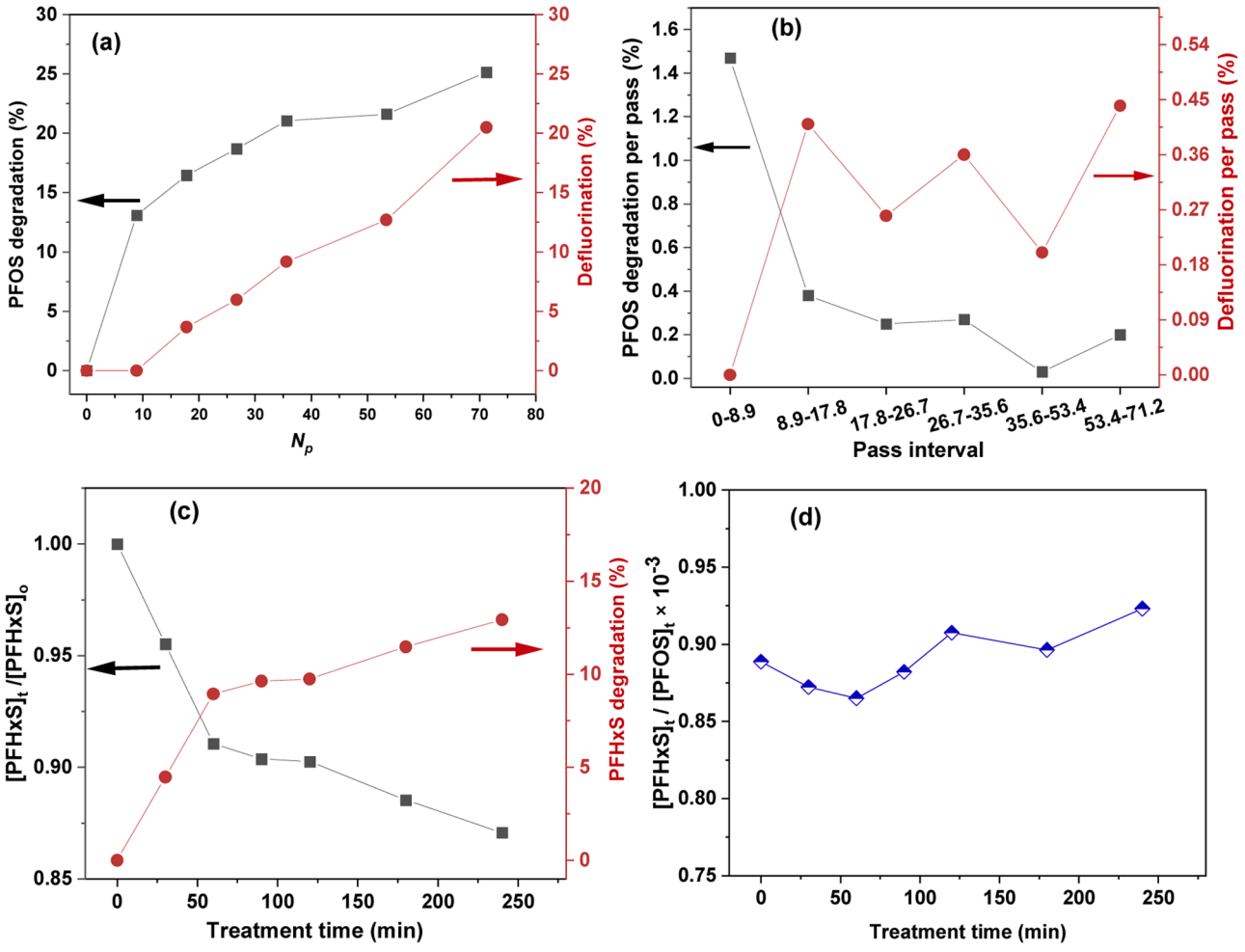

Fig. 3. (a) PFOS degradation and defluorination percentages as a function of N_p. (b) Per-pass degradation and defluorination efficiency. (c) Normalized PFHxS concentration and degradation percentage over treatment time. (d) Concentration ratio (mg/mg) of PFOS to PFHxS over treatment time (at $[PFOS]_o$ = 5 mg/L, $[PFHxS]_o$ = 4 µg/L, Y-axis multiplied by 10^{-3}).

Upon bubble collapse, the resulting intense physicochemical effects can potentially degrade the head groups and cleave the strong C–F bonds in PFOS, thereby contributing to its overall degradation. Cavitation events originating from the orifice are visualized in Supplementary Video.

To evaluate process performance, PFOS degradation and defluorination were plotted as functions of N_p through the HC reactor, as shown in Fig. 3(a). With increasing N_p, PFOS degradation increased steadily and reached about 25%, while defluorination attained about 20% at the highest number of passes. At lower N_p values, PFOS degradation exceeded defluorination, indicating that initial breakdown likely produces intermediate transformation products and/or there is a fraction of PFOS lost due to adsorption to components of the system. In general, low turnover values are related to large relative errors due to the problem of the difference of two large numbers while the formation of fluoride as product is more characteristic. At higher N_p, PFOS degradation ratios are larger and more reliable and under these conditions degradation and defluorination ratios became nearly equal. No shorter-chain perfluorocarboxylates were detected throughout the reaction period, despite the LC–MS detection limit being sufficient to identify products formed at levels as low as 0.05 mol% of the initial PFOS concentration. The high fluoride yield per degraded PFOS molecule, combined with the absence of shorter-chain products in the aqueous phase, indicates that PFOS reaching the cavitation bubble undergoes near-complete mineralization, implying further decomposition of intermediates into fluoride ions. This observation is consistent with previous studies. Wang et al [29] reported 18.9% degradation and 15.8% defluorination of PFOA using HC alone, with no transformation products detected.

In contrast, other oxidation and reduction processes often require significantly longer treatment times to achieve full defluorination and run via step-wise chain-shortening of perfluoroalkyl acids. For example, Deng et al [48] showed that ultrasonic persulfate activation degraded PFOA in biochar within 4 hours, while defluorination reached 99.6% after 10 hours. Guan et al [49] demonstrated complete PFAS degradation using a treatment train of UV/sulfite and electrochemical oxidation, where reductive defluorination alone could not achieve full mineralization, but subsequent electrooxidation enabled complete conversion of perfluorinated intermediates. In contrast, HC-based processes do not produce chain-shortened or partially defluorinated intermediates in the water phase, but instead promote direct removal and near-complete mineralization of PFAS upon the first molecular attack by thermolysis/pyrolysis in the collapsing bubble. While this study cannot provide definitive proof, it offers strong evidence supporting this mechanism, warranting further investigation.

Fig. 3(b) presents the degradation and defluorination per pass, providing a comparative metric well-suited for assessing the performance of various HC systems in pollutant treatment. The highest degradation per pass (up to 1.6%) occurred between 0–8.9 passes, while the highest defluorination per pass (up to 0.44%) was observed between 53.4–71.2 passes. In the previous work, Talabazar et al [28] applied a micro-HC chip reactor and achieved 36.1% removal of 11 long- and short-chain PFAS (ng/L range) in membrane bioreactor (MBR)-treated wastewater over 5 treatment cycles (32.5 min total treatment time, at 17.2 bar). Previous investigations have similarly demonstrated that organic pollutant degradation under HC correlates with the number of passes through the reactor [30,50].

The *HRT*, defined as the exact duration the PFOS solution remained in the HC chamber, was calculated to be 92 min for 71 passes. This corresponds to approximately 1 min per pass within the cavitation chamber, compared to an overall treatment time of 240 min (~3 min per pass, including recirculation).

PFHxS, a shorter-chain PFAS often present as an impurity in PFOS, exhibited distinct behavior under HC treatment. Fig. 3(c) shows the normalized concentration and degradation profile of PFHxS over time. After 240 min, PFOS degradation reached 25%, whereas PFHxS degradation was 14%. The initial PFHxS concentration was approximately 1000 times lower than that of PFOS. The PFOS-to-PFHxS concentration ratio (Fig. 3d) showed a slight increasing trend throughout the treatment. PFHxS is less hydrophobic and adsorbs less readily to interfaces compared to PFOS. Its lower degradation efficiency may be attributed to the shorter perfluorinated chain, which reduces interfacial adsorption and limits access to cavitation zones, thereby slowing pyrolytic decomposition. This observation aligns with Talabazar et al [28], who reported lower PFHxS degradation (1–19%) compared to PFOS (38.8–55.4%) during HC treatment of mixed PFAS at ng/L levels. Similarly, sonochemical cavitation studies by Fernandez et al [51] demonstrated slower PFHxS degradation (2.6 μM F^-/min) versus PFOS (3.5 μM F^-/min), accompanied by lower fluoride release (469 μM vs. 638 μM after 180 min). These findings highlight the influence of molecular structure, initial concentration, and cavitation intensity on PFAS treatment efficiency.

The initial concentration of pollutant molecules can play a critical role in determining degradation efficiency under HC. According to previous HC-based studies, the degradation rate is inversely proportional to the initial concentration of target pollutants [27,28,46,52]. However, these findings are mainly related to target compounds which are reactive towards HO• and other reactive species formed in the process and such behaviour points to radical formation as rate-controlling step. As shown in Fig. 4(a), PFOS degradation proceeded more rapidly at lower initial concentrations, achieving 30% removal after one pass and 37% after two passes. Fig. 4(b) shows that PFOS degradation was higher at the lower initial concentration, whereas defluorination remained nearly unchanged between the two concentrations. The higher apparent removal efficiency observed at 1 mg/L PFOS may be partly attributed to the greater relative contribution of sorption losses, as available surface sites can reach saturation more rapidly at lower PFOS concentrations.

In dilute solutions, adsorption to reactor surfaces or interfaces may therefore contribute more significantly to the observed degradation. In addition, interfacial saturation effects at cavitation bubbles may play an important role. At higher PFOS concentrations, PFOS molecules likely compete for access to the bubble–liquid interface, leading to saturation of the reactive interfacial zone where cavitation-induced pyrolytic degradation occurs. This competition can limit molecular breakdown and subsequent defluorination. Conversely, at lower PFOS concentrations, PFOS molecules can partition more efficiently to these reactive zones, promoting enhanced degradation, while defluorination remains governed by the intrinsic reaction pathways and thus shows only minor variation.. This behavior aligns with earlier findings: Awoyemi et al [53] reported that high initial PFAS concentrations saturate the bubble surface area, hindering further cavitation-driven degradation. A similar kind of behaviour was also observed in the study conducted by Wang et al [29] on PFOA degradation.

3.2. PFOS degradation and defluorination kinetics

The kinetics of PFOS degradation and defluorination were analyzed to understand the rate and efficiency of PFOS breakdown during HC treatment. Fig. 5(a) shows the first-order kinetics of PFOS and the corresponding release of F^- over a treatment period of 0–240 min, starting with an initial PFOS concentration of 5 mg/L. The degradation of PFOS follows a first-order kinetic model ($R^2 = 0.94$), with a rate constant $k_{PFOS} = 0.7 \times 10^{-3}$ 1/min, as indicated by the linear decrease in $\ln([PFOS]_t/[PFOS]_0)$. The degradation kinetics exhibit two distinct phases, although the difference in slope is relatively small. PFOS degradation proceeded with an initially faster phase from 0–120 min, followed by a slower phase from 120–240 min. When a single first-order kinetic model is applied across the entire treatment duration, this transition in reaction behaviour results in a moderate decrease in the overall goodness of fit. This deviation from ideal first-order kinetics is likely due to several factors: reduced mass transfer of PFOS molecules to the bubble–liquid interface at lower concentrations, accumulation of intermediate species that compete for reactive sites, and decreased reactivity as fewer PFOS

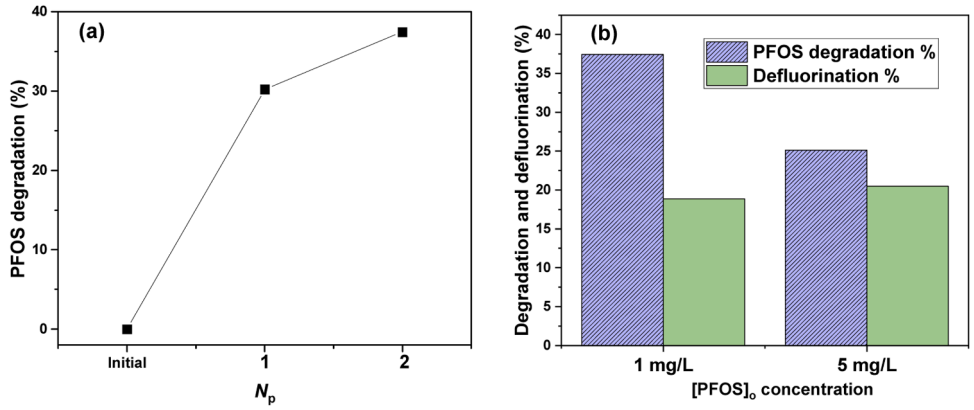

Fig. 4. (a) Normalized PFOS concentration and degradation as a function of the N_p (at [PFOS]$_o$ = 1 mg/L). (b) PFOS degradation and defluorination efficiency at two initial concentrations (at [PFOS]$_o$ = 1 mg/L and 5 mg/L).

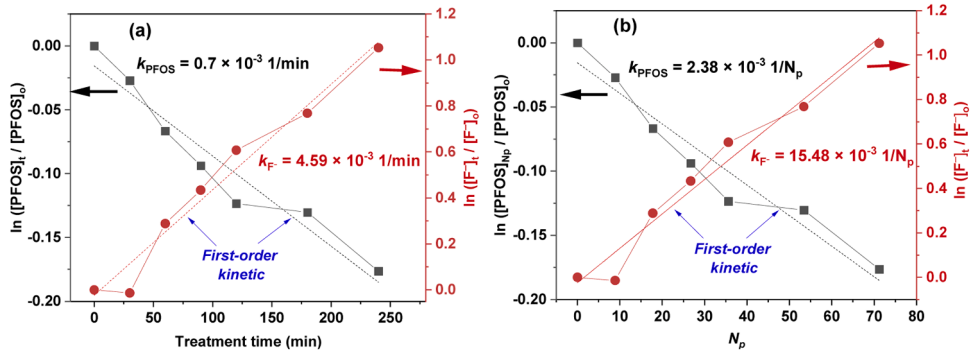

Fig. 5. First order degradation kinetics of PFOS and formation of F$^-$ ions (a) k_1 (1/min) with treatment time. (b) k_2 with 1/N_p (at [PFOS]$_o$ = 5 mg/L).

molecules are available at the cavitation interface during the later stage of treatment.

The formation of F$^-$ also follows first-order kinetics (R^2 = 0.97), with a higher rate constant k_{F^-} = 4.59 × 10^{-3} 1/min. However, it should be noted that in general at low turnover degrees, the concentration-time plots can still give similar good fits with first-order and zero-order kinetics plots. The rapid release of F$^-$ suggests that HC not only breaks down PFOS efficiently but also promotes its mineralization, with fluoride serving as a key indicator of the degradation process. Fig. 5(b) extends the kinetic analysis to N_p, showing that PFOS degradation continues to follow a first-order trend (R^2 = 0.94) with a rate constant k_{PFOS} = 2.38 × 10^{-3} 1/N_p. The generation of F$^-$ increases accordingly, with a rate constant k_{F^-} = 15.48 × 10^{-3} 1/N_p (R^2 = 0.97). More information on the degradation and defluorination kinetics of PFOS achieved in the present study, along with a comparison to existing data on PFOA treatment by HC/persulfate reported by Wang et al [29], is provided in the Supplementary Material (Table A.3).

3.3. Aqueous fluoride ions formation and mass balance

The measurement of aqueous fluoride ions and fluorine mass balance is essential to evaluate the extent of PFOS defluorination and

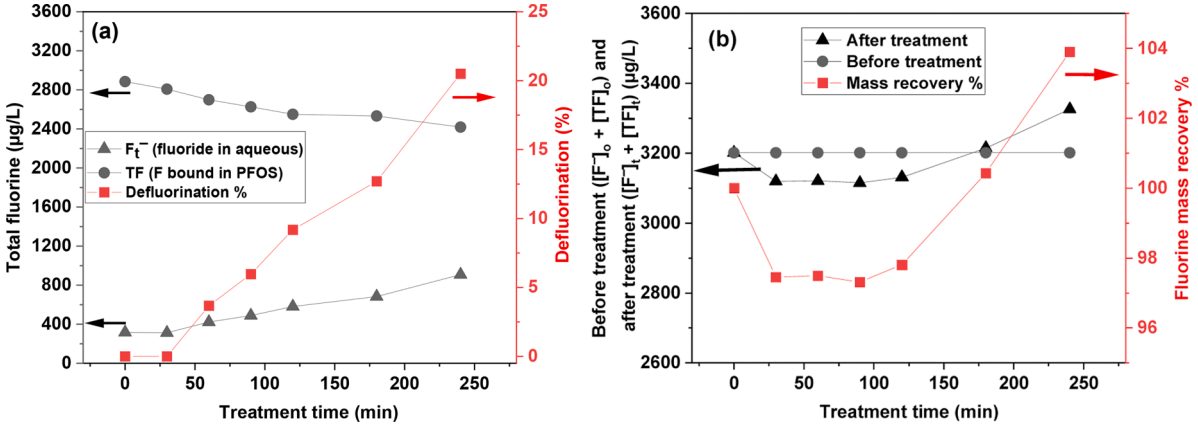

Fig. 6. (a) Concentrations of F$^-$ into the aqueous phase during treatment, fluorine remaining in parent PFOS, and corresponding defluorination percentage. (b) Fluorine mass balance and F$^-$ recovery, calculated from the measured F$^-$ and theoretical total fluorine (TF) from PFOS (organically bound fluorine) at [PFOS]$_o$ = 5 mg/L.

mineralization. Total fluorine was assessed by summing the contributions from both free inorganic fluoride and organically bound fluorine. While free fluoride (released) was directly measured, the fluorine content in parent PFOS was estimated based on measured PFOS concentrations. As shown in Fig. 6(a), over the treatment duration, the concentration of F^- in the aqueous phase increased steadily, indicating progressive defluorination. Simultaneously, the fluorine content associated with PFOS declined, confirming that fluorine was being released from the parent molecule. The defluorination percentage increased proportionally with treatment time, reaching approximately 20% by the end of the process.

Fluctuations in the fluoride mass balance are a common challenge in PFAS degradation studies and may be attributed to incomplete defluorination, analytical limitations in fluoride detection, sorption losses, and the formation of stable fluorinated intermediates [20, 54–56]. Fig. 6(b) compares the total fluorine content before and after treatment calculated as the sum of $[F^-]_t$ and $[TF]_t$ (total fluorine in PFOS) to evaluate mass conservation. While previous reports frequently document mass balance fluctuations in fluoride recovery [20,54–56], we find an almost complete mass balance, thereby validating also the reliability of the quantification methods. Minor deviations observed in the early stages may be attributed to the strong sorption activity of PFOS, which readily adsorbs to system surfaces. Nevertheless, the fluorine mass balance is within 97 to 104% over the whole treatment time, indicating notable accuracy of the methodology. Overall, the mass balance and fluoride release data strongly indicate that HC treatment facilitates both the breakdown and the mineralization of PFOS into CO_2 and F^-.

3.4. Energy requirement for PFOS degradation

The estimation of energy consumption and treatment costs for PFOS removal using HC is critical for assessing the technical and economic feasibility of the process and for enabling meaningful comparisons with previously reported PFAS treatment technologies. In this study, the energy requirements for PFOS degradation were evaluated using multiple performance metrics. These included the amount of PFOS mass removed per unit of energy input (expressed as mg/kWh), the total specific energy consumption normalized to the treated water volume (expressed as kWh/m^3) as well as *EEO* (expressed as kWh/m^3/order). Together, these parameters provide a comprehensive assessment of the energy efficiency of the HC process and its potential applicability for large-scale PFOS remediation.

Fig. 7(a) presents the energy yield (mg PFOS removed per kWh) for both initial concentrations. An inverse relationship was observed: as degradation increased, energy yield decreased. At an initial PFOS concentration of 1 mg/L, the energy yield ranged from 177 to 286 mg/kWh, while at 5 mg/L, it was significantly lower, ranging from 17 to 70 mg/kWh. The energy input in kWh/m^3, as shown in Fig. 7(b), represents the total energy required for PFOS treatment in a tap water matrix.

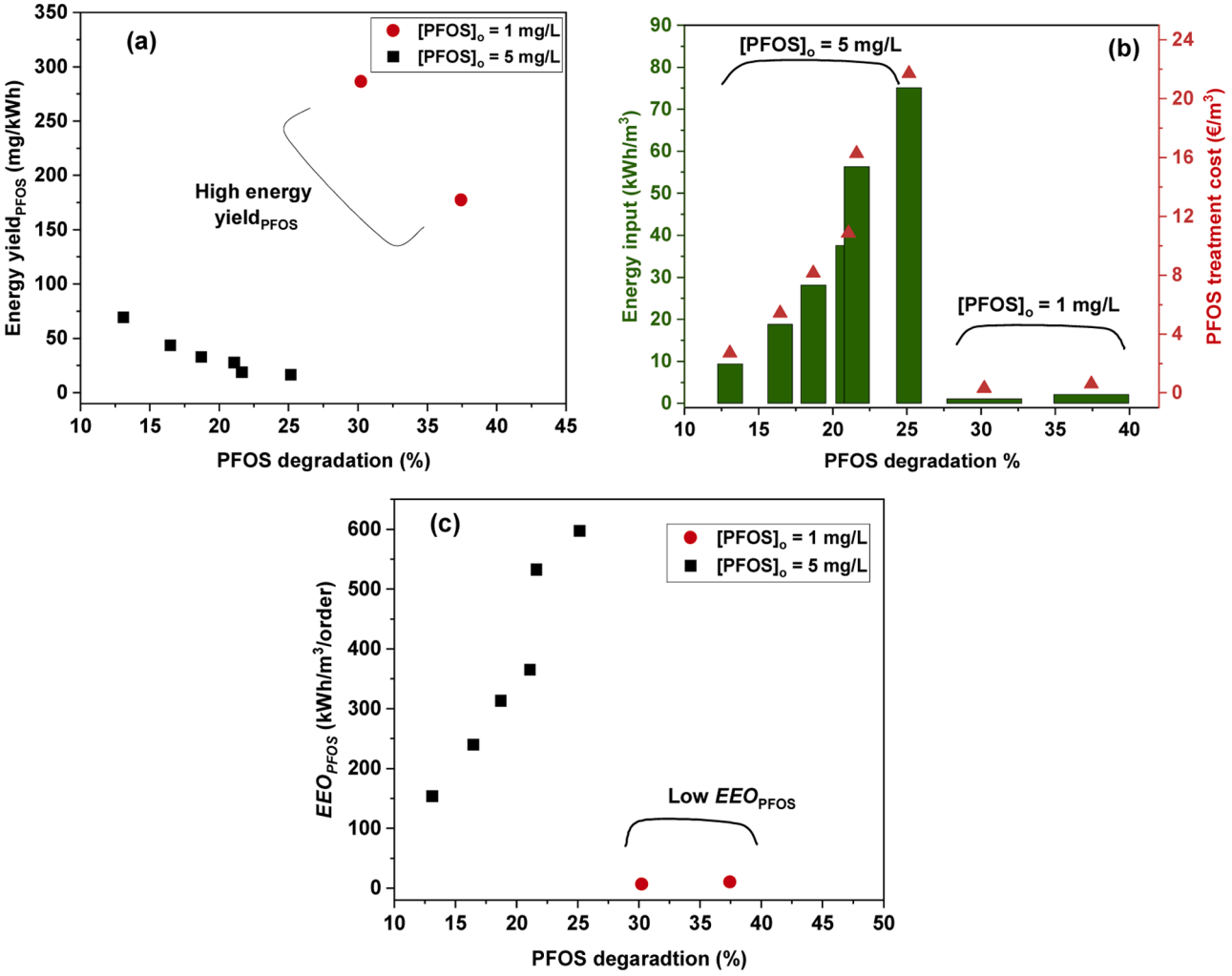

Fig. 7. Energy requirements for PFOS degradation: (a) energy yield versus PFOS degradation, (b) total energy input and corresponding treatment cost versus PFOS degradation, and (c) *EEO* versus PFOS degradation.

Naturally, the water matrix plays a significant role in treatment efficiency. Based on the energy input, the corresponding treatment cost in euros was estimated. At an initial PFOS concentration of 1 mg/L, where lower energy was required, the cost ranged from €0.30 to €0.60/m^3, corresponding to an energy input of 1.05 to 2.11 kWh/m^3. In contrast, for a higher initial concentration of 5 mg/L, the energy demand increased substantially (9 to 75 kWh/m^3), resulting in treatment costs ranging from around €3 to €22/m^3. Overall, the estimated treatment cost using HC ranged from €0.30 to €22/m^3, depending on initial concentration and energy input.

The *EEO* varied with the extent of degradation, as shown in Fig. 7(c). Lower *EEO* values were achieved with fewer passes and lower initial PFOS concentrations. For instance, at an initial concentration of 1 mg/L, the *EEO* ranged from 7 to 10 kWh/m^3/order for degradation levels between 30 % and 37 %. In contrast, at a higher concentration of 5 mg/L, *EEO* values increased substantially, ranging from 154 to 598 kWh/m^3/order for degradation levels between 13% (likely limited by PFOS adsorption) and 25% (approximately 20% defluorination). To evaluate the efficiency of the HC process, these *EEO* values were compared with those reported for other PFOS treatment technologies, as summarized in Table 3. Our calculated *EEO* values (7 to 598 kWh/m^3/order) are generally lower than most of those reported in the literature (see Table 3), suggesting that HC is a relatively energy-efficient treatment method. Notably, even though the HC reactor used in this study has not been fully optimized, its performance is already comparable to, or in some cases better than, other established PFOS degradation technologies. More details are provided in Supplementary Material (Note).

3.5. Possible PFOS mineralization process by hydrodynamic cavitation

In this work, efficient mineralization of PFOS was achieved, as evidenced by the release of F^- ions and the absence of detectable organic intermediates after extended treatment. These results indicate that PFOS was effectively degraded without the accumulation of persistent transformation products. The proposed PFOS degradation pathway under HC conditions is summarized and schematically illustrated in Fig. 8. Upon exposure to HC, PFOS molecules preferentially adsorb at the gas–liquid interface of collapsing cavitation bubbles due to their amphiphilic nature. The extreme local conditions generated during bubble collapse characterized by very high temperatures and pressures provide sufficient energy to initiate molecular bond cleavage. Degradation is expected to begin with cleavage of the sulfonate headgroup, as the C–S bond (bond dissociation energy ~301–355 kJ/mol) is significantly weaker than the C–F bond (~485 kJ/mol). Subsequent degradation and defluorination likely proceed through a combination of radical-mediated reactions and thermal (pyrolytic) decomposition during repeated bubble collapse events. Although no intermediates were detected experimentally, a plausible degradation pathway can be inferred based on PFOS molecular structure and known cavitation chemistry. Fig. 8 therefore presents multiple mechanistic possibilities. One pathway involves transient formation of shorter-chain fluorinated acids, which may be generated but rapidly degraded and thus not detected in the aqueous phase. Alternatively, PFOS molecules may undergo extensive C–C bond scission within the cavitation bubble itself, leading directly to complete mineralization without release of measurable intermediates. Overall, the results suggest that both reactions within the bubble interior and at the bubble–liquid interface contribute to PFOS degradation, ultimately resulting in effective defluorination and mineralization under HC conditions.

Table 3
Comparison of *EEO* and rate constant values from literature and the present work for PFOS degradation methods.

Treatment process	$[PFOS]_o$ concentration (mg/L)	$k_{PFOS} \times 10^{-3}$ (1/min)	$EEO \times 10^3$ (kWh/m^3/order)	References
HC	1 – 5	0.7– 40	0.007 – 0.598	**Present work**
Sonication	0.0029	16	2.900	Kalra et al [57]
Sonication	1	15.3	0.502 – 1.644	Ilić et al [55]
Gliding arc plasma	100	-	0.0232 – 0.2134	Lewis et al [58]
Direct UV	20	0.09	18.19	Yamamoto et al [59]
Sonolysis	10	16	8.0	Moriwaki et al [60]
UV	18.6	15.2	1.27	Lyu et al [61]
Electrochemical oxidation	~ 25	14	-	Luo et al [62]
Plasma	ng/L–mg/L range	-	0.380 – 0.830	
Electrochemical oxidation	-	-	0.005 – 0.132	Sharma et al [43]
Photocatalysis	200	-	9.335	
Electron beam	1	-	0.556	
Photodegradation + boiling	18.6	-	1.177	
Electrochemical oxidation	50	-	0.032	
Heat	100	0.417	64.4	Yang et al [63]
UV	100	0.300	38.4	
Ultrasound	100	0.0833	396.4	

Previous studies have attempted to elucidate PFAS degradation pathways under cavitation-based treatments [28,29,64]. HC alone probably does not release detectable intermediates into the aqueous phase; however, when combined with reagents, such as oxidants, intermediates often appear. For example, Wang et al [29] reported that HC combined with activated persulfate accelerated PFOA removal but generated several short-chain intermediates, including PFHpA, PFHxA, PFPeA, and PFBA. In contrast, HC alone produced no measurable intermediates under the same conditions, suggesting that while the presence of persulfate enhances parent compound removal, it does not guarantee similar fast complete mineralization.

Talabazar et al [28] proposed that PFAS degradation under HC is driven by high-energy pyrolytic and thermolytic events within collapsing bubbles, leading to primary C–F bond cleavage and the generation of F^-. Similarly, Rodríguez-Freire et al [64] observed PFOS degradation via sonochemical cavitation, detecting fluoride and sulfate as major products and suggesting transient short-chain PFAS intermediates. Vecitis et al [41] described a two-step acoustic cavitation mechanism involving PFOS adsorption at the bubble interface followed by pyrolytic decomposition. In the present study, no short-chain perfluorocarboxylates were detected throughout the treatment, despite HPLC–MS detection limits as low as 0.05 mol % of the initial PFOS concentration. This absence suggests either complete degradation of any transient intermediates or concentrations below the current analytical threshold. Future work will employ more sensitive time-resolved and high-resolution techniques to capture low-abundance intermediates and refine the mechanistic understanding of PFOS breakdown under HC.

3.6. Future research direction

In this study, HC alone was able to degrade PFOS at high concentrations, achieving 37% degradation and 20% defluorination at an *EEO* of 10 kWh/m^3/order. Higher removal efficiencies would require longer treatment or multiple passes, but these results are in line with cavitation-alone performance reported in the literature. To further enhance performance, integrating HC with non-condensable gases (e.g., air, oxygen, and argon) is a promising option The use of non-condensable gases plays a crucial role in enhancing local temperature, influencing bubble collapse dynamics, and promoting mass transfer, which together create

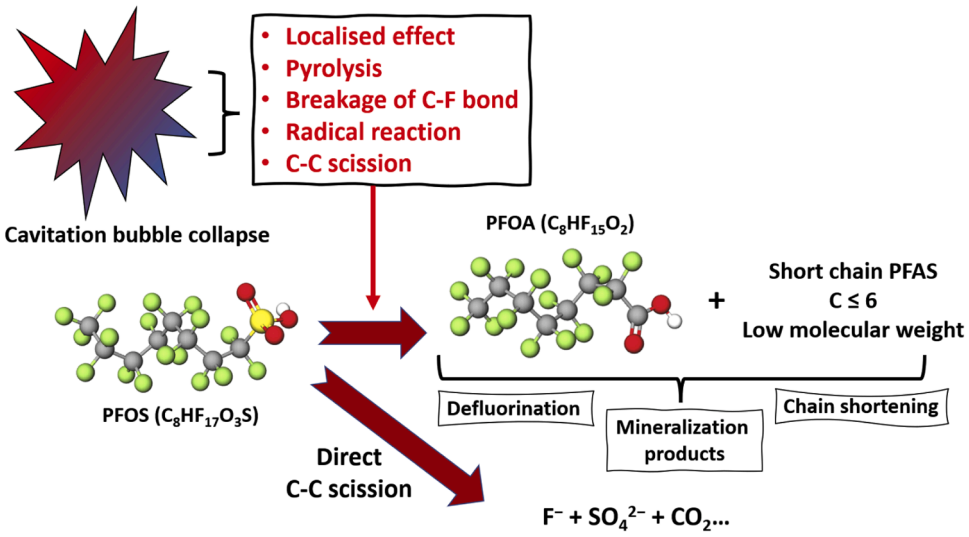

Fig. 8. The possible breakdown mechanism for PFOS under intense HC conditions.

a chemically rich environment for micropollutant degradation in water. Previous studies have shown that noble gases significantly influence cavitation behaviour due to their high adiabatic index (~1.67). For instance, Rooze et al [65] reported that halogenated compounds degrade more efficiently in the presence of argon, while non-halogenated compounds degrade more effectively in air. Additionally, exploring new reactor geometries, such as designs incorporating multiple orifices or nozzles, could further enhance cavitation bubble formation, promote more intense bubble implosion, and create favorable local physicochemical environments, all of which are critical for scalability [27,31].

A single technology is often insufficient due to the limitations of current PFAS removal methods, especially in simultaneously treating ultra-short-, short-, and long-chain PFAS in continuous mode. Therefore, integrating treatment processes or combining two or more techniques offers an opportunity to overcome the shortcomings of individual methods and enhance PFAS elimination efficiency [11,20,66–68]. For example, most existing approaches rely on concentrating PFAS using membrane separation, adsorption, ion-exchange resins, or flotation. In these processes, PFAS is captured but not destroyed, and the concentrated waste must be transported off-site for incineration or other destructive treatment. This not only incurs high transportation and disposal costs but also introduces the risk of generating hazardous waste. As shown in Fig. 9, a treatment chain approach can be adopted: initial physical separation (e.g., using activated carbon, ion-exchange resins, membrane separation or foam fractionation) is followed by on-site PFAS degradation using HC. In the proposed integrated approach, HC can be applied directly to adsorbent regeneration solutions or concentrated retentates, enabling PFAS degradation and mineralization with concurrent defluorination, thereby eliminating the need for off-site incineration. This integrated strategy reduces overall treatment costs and minimizes the risk of secondary contamination. Final polishing steps (e.g. cold atmospheric plasma) may still be required to remove any residual contaminants and ensure compliance with discharge standards [69,70].

4. Conclusions

In this study, an orifice-based HC system was employed for the degradation and defluorination of long-chain persistent PFAS. The treatment was conducted under high initial PFOS concentrations with continuous recirculation and intense cavitation conditions. PFOS degradation under HC followed apparent first-order kinetics, demonstrating effective molecular breakdown and C–F bond cleavage. The release of fluoride ions into the aqueous phase confirmed PFOS mineralization and supports the occurrence of cavitation-induced defluorination rather than mere transformation to stable by-products. While PFOS degradation efficiencies varied with initial concentration, the experiments conducted at 5 mg/L provided more consistent and reliable

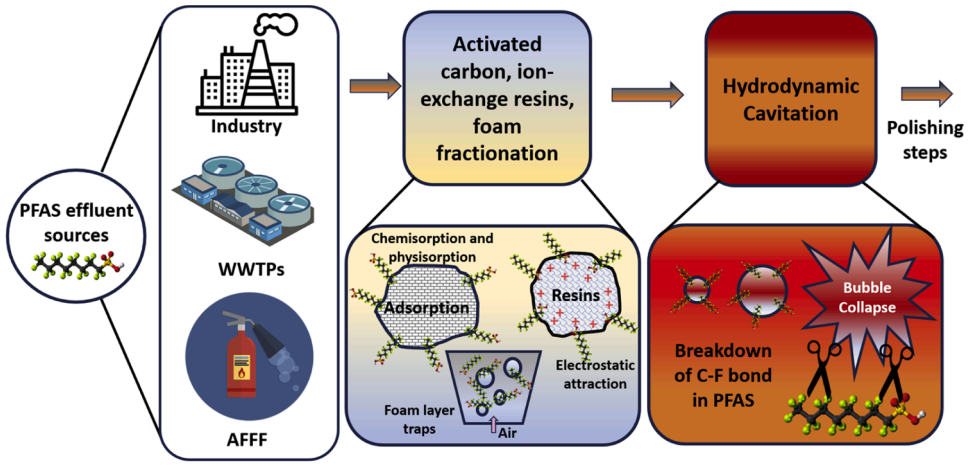

Fig. 9. Treatment chain combining physical separation and degradation processes for PFAS removal in real-world applications.

results, enabling a more robust fluoride mass balance and interpretation of degradation pathways. In contrast, results obtained at lower initial concentrations were subject to greater uncertainty, likely influenced by sorption losses and interfacial effects, which complicate quantitative interpretation. The findings demonstrate the capability of the orifice-based HC system to induce PFOS degradation and defluorination, with the higher-concentration experiments offering stronger evidence for effective destruction rather than incomplete transformation.

The *EEO* ranged from 7 to 598 kWh/m^3/order, while the energy yield varied between 17 and 286 mg/kWh. The overall energy input for PFOS degradation ranged from 1 to 75 kWh/m^3, depending on the initial PFOS concentration and the extent of degradation.. These results indicate that HC enables effective PFOS degradation with lower energy requirements compared to most reported studies and conventional treatment methods. The extreme physicochemical conditions generated during bubble implosion indicate that PFOS reaching the cavitation bubble undergoes near-complete mineralization, with subsequent decomposition of intermediates into fluoride ions.

Overall, this study demonstrates that HC is a promising, non-thermal, energy-efficient, and scalable technology for PFAS degradation. It presents a viable alternative to conventional treatment methods and lays the groundwork for sustainable, large-scale PFAS remediation strategies. Further efforts in optimizing HC reactor geometry and operating conditions are essential to enhance PFAS breakdown and defluorination efficiency, enabling successful upscaling and implementation at diverse sites such as AFFF, industrial facilities and WWTPs.

CRediT authorship contribution statement

Amit Kumar: Writing – review & editing, Writing – original draft, Visualization, Methodology, Investigation, Formal analysis, Conceptualization. **Anett Georgi:** Writing – review & editing, Validation, Resources, Investigation. **Ysabel Huaccallo-Aguilar:** Formal analysis, Investigation, Writing – review & editing. **Markus Meier:** Writing – review & editing, Funding acquisition. **Holger Kryk:** Writing – review & editing. **Sebastian Felix Reinecke:** Writing – review & editing, Validation, Supervision, Resources, Project administration, Formal analysis, Conceptualization. **Uwe Hampel:** Writing – review & editing, Supervision, Resources, Project administration.

Declaration of competing interest

The authors declare that they have no known financial or personal conflicts of interest that could have influenced the work reported in this paper.

Acknowledgments

We extend our sincere thanks to Mr. Mathias Menzel for his technical assistance with the hydrodynamic cavitation setup used in PFAS treatment. We are also grateful to Ms. Heike Schlessiger and Mr. Michael Knobel for their valuable support in preparing the chemical reagents and solutions essential to this study.

Funding information: This research received partial funding from the Initiative and Networking Fund of the Helmholtz Association through the Clean Water Technology Lab (CLEWATEC), a Helmholtz Innovation Lab, under reference number HIL-A02. Additional support was provided by the European Union and co-financed through tax revenues based on the budget passed by the Saxon State Parliament, under the project HyKaPro SAB-EFRE (AN 100689115).

Supplementary materials

Supplementary material associated with this article can be found, in the online version, at doi:10.1016/j.ceja.2026.101046.

Data availability

Data will be made available on request.

References

[1] K. Fu, J. Huang, F. Luo, Z. Fang, D. Yu, X. Zhang, D. Wang, M. Xing, J. Luo, Understanding the selective removal of perfluoroalkyl and polyfluoroalkyl substances via fluorine–fluorine interactions: a critical review, Env. Sci. Technol. (2024), https://doi.org/10.1021/acs.est.4c06519.

[2] S.Y. Wee, A.Z. Aris, Revisiting the "forever chemicals", PFOA and PFOS exposure in drinking water, NPJ. Clean. Water. 6 (2023), https://doi.org/10.1038/s41545-023-00274-6.

[3] D. Ackerman Grunfeld, D. Gilbert, J. Hou, A.M. Jones, M.J. Lee, T.C.G. Kibbey, D. M. O'Carroll, Underestimated burden of per- and polyfluoroalkyl substances in global surface waters and groundwaters, Nat. Geosci. 17 (2024) 340–346, https://doi.org/10.1038/s41561-024-01402-8.

[4] S.C.E. Leung, P. Shukla, D. Chen, E. Eftekhari, H. An, F. Zare, N. Ghasemi, D. Zhang, N.T. Nguyen, Q. Li, Emerging technologies for PFOS/PFOA degradation and removal: a review, Sci. Total. Environ. 827 (2022) 153669, https://doi.org/10.1016/j.scitotenv.2022.153669.

[5] X. Liu, A. Sau, A.R. Green, M.V. Popescu, N.F. Pompetti, Y. Li, Y. Zhao, R.S. Paton, N.H. Damrauer, G.M. Miyake, Photocatalytic C–F bond activation in small molecules and polyfluoroalkyl substances, Nature 637 (2025) 601–607, https://doi.org/10.1038/s41586-024-08327-7.

[6] E.M. Sunderland, X.C. Hu, C. Dassuncao, A.K. Tokranov, C.C. Wagner, J.G. Allen, A review of the pathways of human exposure to poly- and perfluoroalkyl substances (PFASs) and present understanding of health effects, J. Expo. Sci. Env. Epidemiol. 29 (2019) 131–147, https://doi.org/10.1038/s41370-018-0094-1.

[7] D.Q. Andrews, O.V. Naidenko, Population-Wide Exposure to Per- and polyfluoroalkyl substances from drinking water in the United States, Env. Sci. Technol. Lett. 7 (2020) 931–936, https://doi.org/10.1021/acs.estlett.0c00713.

[8] W. Perng, D. Nakiwala, J.M. Goodrich, What happens in utero does not stay in utero: a review of evidence for prenatal epigenetic programming by per- and polyfluoroalkyl substances (PFAS) in infants, children, and adolescents, Curr. Envir. Health Rpt. 10 (2022) 35–44, https://doi.org/10.1007/s40572-022-00387-z.

[9] O.A. Zelekew, Z. Wang, Y. Gu, Y. Wu, Recent progress on photoactive heterogeneous photocatalysts for the degradation of per-and polyfluoroalkyl substances (PFAS): Mechanisms, DFT calculations, limitations, and future prospects, J. Environ. Chem. Eng. 12 (2024) 113323, https://doi.org/10.1016/j.jece.2024.113323.

[10] F. Liu, X. Guan, F. Xiao, Photodegradation of per- and polyfluoroalkyl substances in water: a review of fundamentals and applications, J. Hazard. Mater. 439 (2022) 129580, https://doi.org/10.1016/j.jhazmat.2022.129580.

[11] N. Kim, J. Elbert, E. Shchukina, X. Su, Integrating redox-electrodialysis and electrosorption for the removal of ultra-short- to long-chain PFAS, Nat. Commun. 15 (2024), https://doi.org/10.1038/s41467-024-52630-w.

[12] A.M. Vuong, K. Yolton, C. Xie, K.N. Dietrich, J.M. Braun, G.M. Webster, A. M. Calafat, B.P. Lanphear, A. Chen, Prenatal and childhood exposure to poly- and perfluoroalkyl substances (PFAS) and cognitive development in children at age 8 years, Environ. Res. 172 (2019) 242–248, https://doi.org/10.1016/j.envres.2019.02.025.

[13] V. Polychronidou, R. Nag, Human health risk assessment of Per- and polyfluoroalkyl substances (PFAS), Sci. Total. Environ. 1000 (2025) 180428, https://doi.org/10.1016/j.scitotenv.2025.180428.

[14] M. Grung, D.Ø. Hjermann, T. Rundberget, K. Bæk, C. Thomsen, H.K. Knutsen, L. S. Haug, Low levels of per- and polyfluoroalkyl substances (PFAS) detected in drinking water in Norway, but elevated concentrations found near known sources, Sci. Total. Environ. 947 (2024) 174550, https://doi.org/10.1016/j.scitotenv.2024.174550.

[15] F. Kozisek, D. Dvorakova, F. Kotal, H. Jeligova, L. Mayerova, V. Svobodova, M. Jurikova, V. Gomersall, J. Pulkrabova, Assessing PFAS in drinking water: insights from the Czech Republic's risk-based monitoring approach, Chemosphere 370 (2025) 143969, https://doi.org/10.1016/j.chemosphere.2024.143969.

[16] J. Li, W. Duan, Z. An, Z. Jiang, L. Li, M. Guo, Z. Tan, X. Zeng, X. Liu, Y. Liu, A. Li, H. Guo, Legacy and alternative per- and polyfluoroalkyl substances spatiotemporal distribution in China: human exposure, environmental media, and risk assessment, J. Hazard. Mater. 480 (2024) 135795, https://doi.org/10.1016/j.jhazmat.2024.135795.

[17] S. Yadav, I. Ibrar, R.A. Al-Juboori, L. Singh, N. Ganbat, T. Kazwini, E. Karbassiyazdi, A.K. Samal, S. Subbiah, A. Altaee, Updated review on emerging technologies for PFAS contaminated water treatment, Chem. Eng. Res. Des. 182 (2022) 667–700, https://doi.org/10.1016/j.cherd.2022.04.009.

[18] D.M. Wanninayake, Comparison of currently available PFAS remediation technologies in water: a review, J. Environ. Manag. 283 (2021) 111977, https://doi.org/10.1016/j.jenvman.2021.111977.

[19] J.S. Ko, N.Q. Le, D.R. Schlesinger, D. Zhang, J.K. Johnson, Z. Xia, Novel niobium-doped titanium oxide towards electrochemical destruction of forever chemicals, Sci. Rep. 11 (2021), https://doi.org/10.1038/s41598-021-97596-7.

[20] C.S. Tshangana, S.T. Nhlengethwa, S. Glass, S. Denison, A.T. Kuvarega, T.T. I. Nkambule, B.B. Mamba, P.J.J. Alvarez, A.A. Muleja, Technology status to treat PFAS-contaminated water and limiting factors for their effective full-scale

application, NPJ. Clean. Water. 8 (2025), https://doi.org/10.1038/s41545-025-00457-3.
[21] R.W. Marsh, J.A. Kewalramani, B. Bezerra De Souza, J.N. Meegoda, The use of a fluorine mass balance to demonstrate the mineralization of PFAS by high frequency and high power ultrasound, Chemosphere 352 (2024) 141270, https://doi.org/10.1016/j.chemosphere.2024.141270.
[22] M. Gar Alalm, D.C. Boffito, Mechanisms and pathways of PFAS degradation by advanced oxidation and reduction processes: a critical review, Chem. Eng. J. 450 (2022) 138352, https://doi.org/10.1016/j.cej.2022.138352.
[23] E. Banayan Esfahani, F. Asadi Zeidabadi, S. Zhang, M. Mohseni, Photo-chemical/catalytic oxidative/reductive decomposition of per- and poly-fluoroalkyl substances (PFAS), decomposition mechanisms and effects of key factors: a review, Water Res. Technol. 8 (2022) 698–728, https://doi.org/10.1039/D1EW00774B.
[24] P. Dewapriya, L. Chadwick, S.G. Gorji, B. Schulze, S. Valsecchi, S. Samanipour, K. V. Thomas, S.L. Kaserzon, Per- and polyfluoroalkyl substances (PFAS) in consumer products: current knowledge and research gaps, J. Hazard. Mater. Lett. 4 (2023) 100086, https://doi.org/10.1016/j.hazl.2023.100086.
[25] G. Li, M. Peng, Q. Huang, C.H. Huang, Y. Chen, G. Hawkins, K. Li, A review on the recent mechanisms investigation of PFAS electrochemical oxidation degradation: mechanisms, DFT calculation, and pathways, Front. Env. Eng. 4 (2025) 1568542, https://doi.org/10.3389/fenve.2025.1568542.
[26] B. Chan, L. Radom, Hierarchy of relative bond dissociation enthalpies and their use to efficiently compute accurate absolute bond dissociation enthalpies for C–H, C–C, and C–F bonds, J. Phys. Chem. A 117 (2013) 3666–3675, https://doi.org/10.1021/jp401248r.
[27] Y. Song, R. Hou, W. Zhang, J. Liu, Hydrodynamic cavitation as an efficient water treatment method for various sewage:- a review, Water. Sci. Technol. 86 (2022) 302–320, https://doi.org/10.2166/wst.2022.201.
[28] F. Rokhsar Talabazar, C. Baresel, R. Ghorbani, I. Tzanakis, A. Koşar, D. Grishenkov, M. Ghorbani, Removal of per- and polyfluoroalkyl substances (PFAS) from wastewater using the hydrodynamic cavitation on a chip concept, Chem. Eng. J. 495 (2024) 153573, https://doi.org/10.1016/j.cej.2024.153573.
[29] X. Wang, M. Wang, G. Yu, W. Wang, H. Liu, Z. Chen, H. Chen, Breakdown of PFOA in a hydrodynamic cavitation-activated persulfate system: comparative roles of sulfate and hydroxyl radicals in degradation process and mechanistic insights, J. Environ. Chem. Eng. 12 (2024) 113376, https://doi.org/10.1016/j.jece.2024.113376.
[30] B. Wang, H. Su, B. Zhang, Hydrodynamic cavitation as a promising route for wastewater treatment – a review, Chem. Eng. J. 412 (2021) 128685, https://doi.org/10.1016/j.cej.2021.128685.
[31] R. Shokoohi, A. Rahmani, G. Asgari, M. Ashrafi, E. Ghahramani, The effect of the combined system of hydrodynamic cavitation, ozone, and hydrogen peroxide on chlorophyll a and organic substances removal in the raw water, Sci. Rep. 13 (2023), https://doi.org/10.1038/s41598-023-37167-0.
[32] Y. Huaccallo-Aguilar, A. Kumar, M. Meier, A. Lerch, S.F. Reinecke, Efficient removal of succinic acid by continuous hydrodynamic cavitation combined with ozone and side influent injection, J. Environ. Manag. 370 (2024) 122795, https://doi.org/10.1016/j.jenvman.2024.122795.
[33] A. Kumar, Y. Huaccallo-Aguilar, J. Schäfer, M. Meier, W. Ding, S.F. Reinecke, U. Hampel, Pilot-scale hydrodynamic cavitation-enhanced ozonation for efficient removal of persistent pharmaceuticals from aqueous matrices: experimental and numerical simulation studies, Sep. Purif. Technol. 378 (2025) 134558, https://doi.org/10.1016/j.seppur.2025.134558.
[34] F. Hong, H. Xue, X. Yuan, L. Wang, H. Tian, L. Ye, J. Jia, D. Ying, Y. Huang, Numerical investigation on the hydrodynamic performance with special emphasis on the cavitation intensity detection in a Venturi cavitator, Process. Saf. Environ. Prot. 175 (2023) 212–226, https://doi.org/10.1016/j.psep.2023.05.037.
[35] G.G. Dastane, H. Thakkar, R. Shah, S. Perala, J. Raut, A.B. Pandit, Single and multiphase CFD simulations for designing cavitating venturi, Chem. Eng. Res. Des. 149 (2019) 1–12, https://doi.org/10.1016/j.cherd.2019.06.036.
[36] W. Ding, D. Ying, F. Hong, S.N. Khan, Y. Huang, J. Jia, Establishment and validation of a multiscale hydrodynamic cavitation model for radical yield: new insights into optimal pressure phenomenon, Sep. Purif. Technol. 379 (2025) 135187, https://doi.org/10.1016/j.seppur.2025.135187.
[37] W. Ding, F. Hong, D. Ying, Y. Huang, S. Nawaz Khan, J. Jia, A comprehensive study on the effects of annular protrusion for cavitation intensification in Venturi tubes, Chem. Eng. J. 498 (2024) 155306, https://doi.org/10.1016/j.cej.2024.155306.
[38] K. Yasui, The reducing agents in sonochemical reactions without any additives, Molecules 28 (2023) 4198, https://doi.org/10.3390/molecules28104198.
[39] K. Fattahi, D.C. Boffito, E. Robert, Quantifying the chemical activity of cavitation bubbles in a cluster, Sci. Rep. 14 (2024) 7978, https://doi.org/10.1038/s41598-024-56906-5.
[40] B. Bezerra De Souza, J.A. Kewalramani, R.W. Marsh, J. Meegoda, Molecular dynamics simulation of the impact of functional head groups and chain lengths of PFAS degradation using ultrasound technology, Water 17 (2025) 1025, https://doi.org/10.3390/w17071025.
[41] C.D. Vecitis, H. Park, J. Cheng, B.T. Mader, M.R. Hoffmann, Enhancement of Perfluorooctanoate and Perfluorooctanesulfonate activity at acoustic cavitation bubble interfaces, J. Phys. Chem. C 112 (2008) 16850–16857, https://doi.org/10.1021/jp804050p.
[42] S. Puttamreddy, N. Nippatlapalli, Advanced insights into sustainable electrooxidation technique and futuristic strategies: multifaceted approach for PFAS degradation, J. Environ. Chem. Eng. 12 (2024) 113307, https://doi.org/10.1016/j.jece.2024.113307.
[43] S. Sharma, N.P. Shetti, S. Basu, M.N. Nadagouda, T.M. Aminabhavi, Remediation of per- and polyfluoroalkyls (PFAS) via electrochemical methods, Chem. Eng. J. 430 (2022) 132895, https://doi.org/10.1016/j.cej.2021.132895.
[44] B.C. Kelly, M.G. Ikonomou, J.D. Blair, B. Surridge, D. Hoover, R. Grace, F.A.P. C. Gobas, Perfluoroalkyl contaminants in an arctic marine food web: trophic magnification and wildlife exposure, Env. Sci. Technol. 43 (2009) 4037–4043, https://doi.org/10.1021/es9003894.
[45] M.E. Dimitrakopoulou, M. Karvounis, G. Marinos, Z. Theodorakopoulou, E. Aloizou, G. Petsangourakis, M. Papakonstantinou, G. Stoitsis, Comprehensive analysis of PFAS presence from environment to plate, NPJ. Sci. Food 8 (2024), https://doi.org/10.1038/s41538-024-00319-1.
[46] B. Wang, H. Su, B. Zhang, Hydrodynamic cavitation as a promising route for wastewater treatment – a review, Chem. Eng. J. 412 (2021) 128685, https://doi.org/10.1016/j.cej.2021.128685.
[47] Y. Patil, S.H. Sonawane, P. Shyam, X. Sun, S. Manickam, Hybrid hydrodynamic cavitation (HC) technique for the treatment and disinfection of lake water, Ultrason. Sonochem. 97 (2023) 106454, https://doi.org/10.1016/j.ultsonch.2023.106454.
[48] J. Deng, Y. Fang, C. Hou, Y. Zhang, M. Li, J. Han, W. Du, C. Tang, X. Hu, Ultrasonic assisted activation of persulfate for the treatment of spent porous biochar: degradation of adsorbed PFOA and adsorbent regeneration, J. Environ. Chem. Eng. 11 (2023) 111146, https://doi.org/10.1016/j.jece.2023.111146.
[49] Y. Guan, Z. Liu, N. Yang, S. Yang, L.E. Quispe-Cardenas, J. Liu, Y. Yang, Near-complete destruction of PFAS in aqueous film-forming foam by integrated photo-electrochemical processes, Nat. Water 2 (2024) 443–452, https://doi.org/10.1038/s44221-024-00232-7.
[50] A. Mukherjee, A. Mullick, S. Moulik, A. Roy, Oxidative degradation of emerging micropollutants induced by rotational hydrodynamic cavitating device: a case study with ciprofloxacin, J. Environ. Chem. Eng. 9 (2021) 105652, https://doi.org/10.1016/j.jece.2021.105652.
[51] N.A. Fernandez, L. Rodriguez-Freire, M. Keswani, R. Sierra-Alvarez, Effect of chemical structure on the sonochemical degradation of perfluoroalkyl and polyfluoroalkyl substances (PFASs), Env. Sci.: Water Res. Technol. 2 (2016) 975–983, https://doi.org/10.1039/c6ew00150e.
[52] S. Rajoriya, S. Bargole, V.K. Saharan, Degradation of a cationic dye (Rhodamine 6G) using hydrodynamic cavitation coupled with other oxidative agents: reaction mechanism and pathway, Ultrason. Sonochem. 34 (2017) 183–194, https://doi.org/10.1016/j.ultsonch.2016.05.028.
[53] O.S. Awoyemi, Y. Luo, J. Niu, R. Naidu, C. Fang, Ultrasonic degradation of per-and polyfluoroalkyl substances (PFAS), aqueous film-forming foam (AFFF) and foam fractionate (FF), Chemosphere 360 (2024) 142420, https://doi.org/10.1016/j.chemosphere.2024.142420.
[54] R.K. Singh, N. Multari, C. Nau-Hix, S. Woodard, M. Nickelsen, S. Mededovic Thagard, T.M. Holsen, Removal of poly- and per-fluorinated compounds from ion exchange regenerant still bottom samples in a plasma reactor, Env. Sci. Technol. 54 (2020) 13973–13980, https://doi.org/10.1021/acs.est.0c02158.
[55] N. Ilić, A. Andalib, T. Lippert, O. Knoop, M. Franke, P. Bräutigam, J.E. Drewes, U. Hübner, Ultrasonic degradation of GenX (HFPO-DA) – performance comparison to PFOA and PFOS at high frequencies, Chem. Eng. J. 472 (2023) 144630, https://doi.org/10.1016/j.cej.2023.144630.
[56] A. Fenti, Y. Jin, A.J.H. Rhoades, G.P. Dooley, P. Iovino, S. Salvestrini, D. Musmarra, S. Mahendra, G.F. Peaslee, J. Blotevogel, Performance testing of mesh anodes for in situ electrochemical oxidation of PFAS, Chem. Eng. J. Adv. 9 (2022) 100205, https://doi.org/10.1016/j.ceja.2021.100205.
[57] S. Singh Kalra, B. Cranmer, G. Dooley, A.J. Hanson, S. Maraviov, S.K. Mohanty, J. Blotevogel, S. Mahendra, Sonolytic destruction of Per- and polyfluoroalkyl substances in groundwater, aqueous film-forming Foams, and investigation derived waste, Chem. Eng. J. 425 (2021) 131778, https://doi.org/10.1016/j.cej.2021.131778.
[58] A.J. Lewis, T. Joyce, M. Hadaya, F. Ebrahimi, I. Dragiev, N. Giardetti, J. Yang, G. Fridman, A. Rabinovich, A.A. Fridman, E.R. McKenzie, C.M. Sales, Rapid degradation of PFAS in aqueous solutions by reverse vortex flow gliding arc plasma, Env. Sci.: Water Res. Technol. 6 (2020) 1044–1057, https://doi.org/10.1039/c9ew01050e.
[59] T. Yamamoto, Y. Noma, S. Sakai, Y. Shibata, Photodegradation of perfluorooctane sulfonate by UV irradiation in water and alkaline 2-propanol, Env. Sci. Technol. 41 (2007) 5660–5665, https://doi.org/10.1021/es0706504.
[60] H. Moriwaki, Y. Takagi, M. Tanaka, K. Tsuruho, K. Okitsu, Y. Maeda, Sonochemical decomposition of perfluorooctane sulfonate and perfluorooctanoic acid, Env. Sci. Technol. 39 (2005) 3388–3392, https://doi.org/10.1021/es040342v.
[61] X.J. Lyu, W.W. Li, P.K.S. Lam, H.Q. Yu, Boiling significantly promotes photodegradation of perfluorooctane sulfonate, Chemosphere 138 (2015) 324–327, https://doi.org/10.1016/j.chemosphere.2015.06.027.
[62] Y. Luo, O.S. Awoyemi, S. Gopalan, A. Nolan, F. Robinson, J. Fenstermacher, L. Xu, J. Niu, M. Megharaj, R. Naidu, C. Fang, Investigating the effect of polarity reversal of the applied current on electrochemical degradation of per-and polyfluoroalkyl substances, J. Clean. Prod. 433 (2023) 139691, https://doi.org/10.1016/j.jclepro.2023.139691.
[63] L. Yang, L. He, J. Xue, Y. Ma, Z. Xie, L. Wu, M. Huang, Z. Zhang, Persulfate-based degradation of perfluorooctanoic acid (PFOA) and perfluorooctane sulfonate (PFOS) in aqueous solution: review on influences, mechanisms and prospective, J. Hazard. Mater. 393 (2020) 122405, https://doi.org/10.1016/j.jhazmat.2020.122405.
[64] L. Rodriguez-Freire, R. Balachandran, R. Sierra-Alvarez, M. Keswani, Effect of sound frequency and initial concentration on the sonochemical degradation of

perfluorooctane sulfonate (PFOS), J. Hazard. Mater. 300 (2015) 662–669, https://doi.org/10.1016/j.jhazmat.2015.07.077.
[65] J. Rooze, E.V. Rebrov, J.C. Schouten, J.T.F. Keurentjes, Dissolved gas and ultrasonic cavitation – a review, Ultrason. Sonochem. 20 (2013) 1–11, https://doi.org/10.1016/j.ultsonch.2012.04.013.
[66] F.A. Zeidabadi, E.B. Esfahani, M. Mohseni, Effects of water matrix on per- and polyfluoroalkyl substances (PFAS) treatment: physical-separation and degradation processes – a review, J. Hazard. Mater. Adv. 10 (2023) 100322, https://doi.org/10.1016/j.hazadv.2023.100322.
[67] C.J. Liu, G. McKay, D. Jiang, R. Tenorio, J.T. Cath, C. Amador, C.C. Murray, J. B. Brown, H.B. Wright, C. Schaefer, C.P. Higgins, C. Bellona, T.J. Strathmann, Pilot-scale field demonstration of a hybrid nanofiltration and UV-sulfite treatment train for groundwater contaminated by per- and polyfluoroalkyl substances (PFASs), Water. Res. 205 (2021) 117677, https://doi.org/10.1016/j.watres.2021.117677.
[68] B.M. Aumeier, A. Georgi, N. Saeidi, G. Sigmund, Is sorption technology fit for the removal of persistent and mobile organic contaminants from water? Sci. Total. Environ. 880 (2023) 163343 https://doi.org/10.1016/j.scitotenv.2023.163343.
[69] B. Topolovec, O. Jovanovic, N. Puac, N. Skoro, E.C. Lumbaque, M. Petrovic, Plasma water treatment for PFAS: study of degradation of perfluorinated substances and their byproducts by using cold atmospheric pressure plasma jet, J. Environ. Chem. Eng. 12 (2024) 112979, https://doi.org/10.1016/j.jece.2024.112979.
[70] A. Kumar, N. Škoro, W. Gernjak, N. Puač, Cold atmospheric plasma technology for removal of organic micropollutants from wastewater—a review, Eur. Phys. J. D 75 (2021) 283, https://doi.org/10.1140/epjd/s10053-021-00283-5.